A national laboratory of the U.S. Department of Energy
Office of Energy Efficiency & Renewable Energy

National Renewable Energy Laboratory

Innovation for Our Energy Future

Spectral Content and Spatial Scales in Unsteady Rotationally Augmented Flow Fields

Preprint

S.J. Schreck

To be presented at the EAWE 2007 Torque from Wind Conference
Technical University of Denmark
Lyngby, Denmark
August 28–31, 2007

Conference Paper
NREL/CP-500-41744
August 2007

NREL is operated by Midwest Research Institute ● Battelle Contract No. DE-AC36-99-GO10337

NOTICE

The submitted manuscript has been offered by an employee of the Midwest Research Institute (MRI), a contractor of the US Government under Contract No. DE-AC36-99GO10337. Accordingly, the US Government and MRI retain a nonexclusive royalty-free license to publish or reproduce the published form of this contribution, or allow others to do so, for US Government purposes.

This report was prepared as an account of work sponsored by an agency of the United States government. Neither the United States government nor any agency thereof, nor any of their employees, makes any warranty, express or implied, or assumes any legal liability or responsibility for the accuracy, completeness, or usefulness of any information, apparatus, product, or process disclosed, or represents that its use would not infringe privately owned rights. Reference herein to any specific commercial product, process, or service by trade name, trademark, manufacturer, or otherwise does not necessarily constitute or imply its endorsement, recommendation, or favoring by the United States government or any agency thereof. The views and opinions of authors expressed herein do not necessarily state or reflect those of the United States government or any agency thereof.

Available electronically at http://www.osti.gov/bridge

Available for a processing fee to U.S. Department of Energy
and its contractors, in paper, from:
U.S. Department of Energy
Office of Scientific and Technical Information
P.O. Box 62
Oak Ridge, TN 37831-0062
phone: 865.576.8401
fax: 865.576.5728
email: mailto:reports@adonis.osti.gov

Available for sale to the public, in paper, from:
U.S. Department of Commerce
National Technical Information Service
5285 Port Royal Road
Springfield, VA 22161
phone: 800.553.6847
fax: 703.605.6900
email: orders@ntis.fedworld.gov
online ordering: http://www.ntis.gov/ordering.htm

Printed on paper containing at least 50% wastepaper, including 20% postconsumer waste

Spectral Content and Spatial Scales in Unsteady Rotationally Augmented Flow Fields

Scott Schreck

NREL's National Wind Technology Center
1617 Cole Boulevard
Golden, Colorado 80401
United States

scott_schreck@nrel.gov

Abstract. Frequency spectra were computed from C_n time series acquired during the NASA Ames wind tunnel experiment, for rotationally augmented flow field conditions at zero yaw. Prominent peaks were present in the frequency spectra, corresponding to dominant aerodynamic shedding modes. These shedding modes were well correlated with flow field mean structure, and Strouhal number analyses furnished information regarding time varying flow field kinematics. Specifically, Strouhal number analyses implied that one of two distinct shedding modes was present, depending upon test section speed and local inflow angle. Information regarding these shedding kinematics will help provide understanding of the aerodynamics responsible for unsteady load production during rotationally augmented conditions. This, in turn, will aid in establishing a reliable physical basis for accurately predicting the time varying aerodynamic forces responsible for wind turbine fatigue loads and damage.

1. Nomenclature

C_n	normal force coefficient
c_p	pressure coefficient ($(p-p_\infty)/q$)
c	blade chord (m)
f	shedding frequency (Hz)
h	blade projected frontal height (m)
LFA	local inflow angle (deg)
p	static pressure (Pa)
p_∞	freestream static pressure (Pa)
q	dynamic pressure (Pa)
r	radial distance from hub (m)
R	blade length (m)
RPM	revolutions/minute
St	Strouhal number ($f\,h/U_{loc}$)
U_∞	test section speed (m/s)
U_{loc}	local inflow speed (m/s)
Ω	blade rotation rate (rad/s)

2. Introduction

Wind turbine aerodynamics remains a challenging and crucial research area for wind energy. Clearly, steady-state aerodynamic performance is essential to turbine energy capture, since blade aerodynamic forces produce mechanical energy that is subsequently converted to electrical energy. However, deeper inquiry has focused on adverse time varying aerodynamic loads that wind turbines frequently suffer during routine service. These time varying loads can be generated by dynamic stall during operation in yaw, or in significant vertical or horizontal inflow shears. More recently, spontaneous time varying aerodynamic loads have been observed for zero yaw operation in steady, uniform inflow, as described in more detail below. These undesirable aerodynamic loads impose excessive stresses on turbine blades and gear boxes, and appreciably shorten machine service life.

Wind turbine blade aerodynamic phenomena can be broadly categorized according to the operating state of the machine. At zero and low rotor yaw angles, rotational augmentation dominates blade aerodynamic response. As described herein, the spatial and temporal attributes of the structures and processes present in these flow fields hold important implications for load predictions for turbine design and analysis, as well as active aerodynamic control methodologies currently being considered for wind turbine applications.

Augmentation of rotating blade aerodynamic properties, including stall delay and lift enhancement, was first observed for airplane propellers and qualitatively explained in terms of centrifugal and Coriolis accelerations.[1] Some time later, analytical modeling quantitatively accounted for key elements of the rotating blade flow field.[2]

Subsequent rotational augmentation research was carried out for helicopter rotors. Analytical modeling determined that rotationally induced cross flows played an important role in blade lift production.[3] Experimental research [4] suggested that centrifugal forces are important in the presence of flow separation, but of limited influence otherwise.

Prior research concerning rotational augmentation of airplane propeller and helicopter rotor aerodynamics aided later work aimed at wind turbines. However, wind turbines extract energy from flowing air, while propellers and rotors inject energy. This key distinction pointed out the need for rotational augmentation research specific to wind turbines.

Early wind turbine field testing aimed at rotational augmentation affirmed the importance of blade geometry with respect to rotational influences.[5] A wind tunnel experiment showed that blade geometry coupled with blade rotation maintained blade lift under conditions in which lift otherwise would significantly decline.[6] Subsequent wind tunnel research determined that rotational augmentation was most active at the inboard portion of the turbine blade.[7] Concurrent analytical modeling of rotational augmentation has furnished better comprehension of the aerodynamics underlying this phenomenon, and provided basic predictive capabilities for design and analysis.[8-13]

More recently, analysis of turbine aerodynamics measurements acquired during controlled wind tunnel experiments, in conjunction with validated computational results, have provided key physical insights regarding time-averaged characteristics of rotationally augmented flow fields.[14-18] Other studies have concentrated on the time-varying attributes of these flows, quantifying unsteadiness intensity, and relating changes in intensity to mean flow field structures and dimensions. [19,20]

Though aggregate unsteadiness intensity has been quantified for rotationally augmented flows, the spectral constituents and associated flow physics remain unexamined. This and related information will be important for understanding the inherent aerodynamics responsible for this unsteadiness. In turn, this physical information is likely to be helpful in validating computational predictions of these flow phenomena, and for resolving related numerical issues. Together, these complementary elements will form the basis for understanding and predicting the unsteady aerodynamic forces responsible for fatigue loads and damage.

3. Experimental procedures

All surface pressure data used in the current work were acquired during wind tunnel testing of the NREL UAE (National Renewable Energy Laboratory Unsteady Aerodynamics Experiment) horizontal

axis wind turbine. This machine evolved through several phases of field testing, all of which have been documented in detail.[21-24] Subsequently, several UAE configurations were tested in the NASA Ames 80 ft x 120 ft wind tunnel, and are described by Hand, et al.[25]

3.1 Turbine and blades

Data analyzed in the current work were acquired from a two bladed upwind rotor, 10.1 m in diameter, with zero cone angle. The rotor turned counterclockwise (viewed from upwind) at a constant Ω = 72 RPM, was stall regulated, and had a maximum rated power of 19.8 kW. A cylindrical tower 0.4 m in diameter supported the turbine at a hub height of 12.2 m (test section centerline), with 1.32 m rotor overhang. This UAE configuration is depicted in Figure 1.

The blades used throughout the NASA Ames wind tunnel test were both twisted and tapered. Blade taper distribution is apparent in Figure 2, with chord tapering from 0.737 m at 0.25R to 0.356 m at the tip. Blade section twist decreased from 22.1° at 0.25R to 0.0° at the tip. Between 0.25R and the tip, blade cross-section was uniform, corresponding to the S809 airfoil. The airfoil section at 0.25R was joined to the pitch shaft section at 0.12R using linear segments to yield an uninterrupted transition between these two disparate contours. The blade pitched about an axis located 0.30c aft of the leading edge, and centered between the blade upper and lower surfaces at that chord location. The UAE Phase VI blades possessed extremely high structural stiffness, to minimize aerostructural coupling. Design procedures, constraints, and measures of merit for this blade have been documented in detail.[25,26]

Figure 1. UAE wind turbine mounted in the NASA Ames 80 ft x 120 ft wind tunnel.

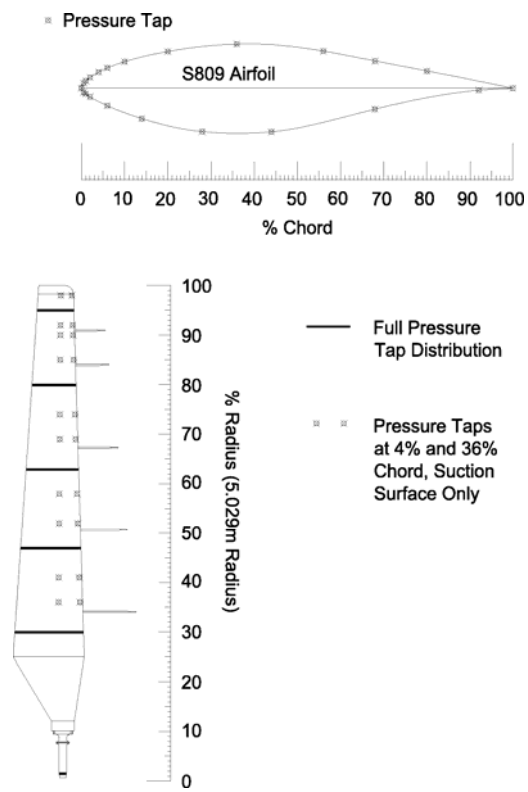

Figure 2. Blade cross-section and planform, showing pressure tap locations.

3.2 Surface pressure and local inflow instrumentation

The black blade shown in Figure 1 was equipped with pressure taps at the locations indicated in Figure 2 to acquire detailed surface pressure data. A full pressure tap distribution consisted of 22 taps distributed on the airfoil section as shown in the upper portion of Figure 2. At the full distributions,

taps were more densely distributed near the blade leading edge to better resolve the steep gradients typically present there, as well as the small structures that initiate there during dynamic stall.

Pressure taps were flush mounted at the blade surface, and had inside diameters of 0.69 mm. From the taps, stainless steel hypodermic tubes having inside diameters of 0.69 mm transmitted the surface pressures to the pressure transducers. Hypodermic tubing lengths were minimized to mitigate pressure delay and dispersion effects. Pressures were measured by five Pressure Systems Incorporated ESP-32 electronically scanned pressure transducers located inside the blade near the five full pressure tap distributions. Each of the transducer pressure inputs was scanned at 520.8 Hz. In conjunction with the tubing frequency response, this provided antialiased digitization and minimal gain variation out to 55 Hz.[21] Time records of c_p were integrated over the sectional chord to obtain time records of C_n.[25] Test section flow speed and air properties were measured using the NASA Ames 80 ft x 120 ft wind tunnel air data system described by Zell.[27]

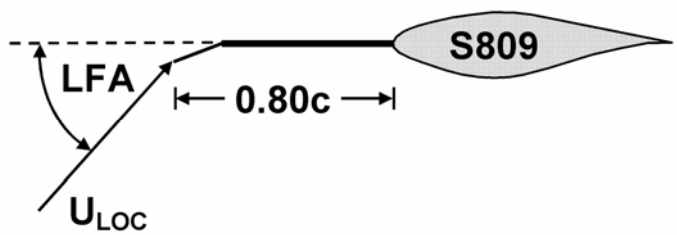

Figure 3. Definition of local inflow angle (LFA).

Local inflow angles were measured near the five full pressure tap distributions using five-hole probes. Probes were mounted on cylindrical stalks at 0.34R, 0.51R, 0.67R, 0.84R, and 0.91R, with the probe tip 0.80c upstream of the blade leading edge. Probes were angled 20° downward relative to the local chord line, allowing measurement of local inflow angles between –20° and 60°. Five-hole probe pressures were measured using the ESP-32 transducers described above, and local inflow angle (LFA) was derived from these measurements. LFA was defined as the angle between the local inflow vector (U_{loc}) and the local blade chord line, measured at the probe tip, as depicted in Figure 3. LFA was defined in a plane parallel to the local chord line and orthogonal to the blade axis.

3.3 Data acquisition protocol

All data used in the current work were collected with the rotor turning at 71.6 RPM. Turbine blade plane of rotation was maintained orthogonal to the test section centerline, yielding $\gamma = 0°$. Blade pitch angle was held constant at 3.0°. U_∞ was varied between 5 m/s and 25 m/s, in nominal 1 m/s increments. At each U_∞, a data record of 30 s duration was acquired, equal to 36 blade rotations.

The zero yaw experiments were carried out twice, corresponding to two separate test sequences (Sequences H and S). Initially, the five-hole probes and stalks were mounted on the blade, and LFA was measured concurrently with other blade aerodynamic properties (Sequence H). Later, the probes and stalks were removed, yielding a 'clean' blade with a flow field free of any disruptions due to the stalks or probes (Sequence S). Measurements then were repeated using this ‘clean’ blade for virtually identical inflow conditions. Overall, this approach allowed accurate measurement of LFA, provided a blade flow field free of intrusions, and allowed for assessment of flow field stability and repeatability.

3.4 Inflow angle and force nondimensionalization

Derivation of angle of attack and lift coefficient for rotating blades using measurements on or near the blade remains a challenging and essential area of inquiry [5,7,28-32]. However, in the current work, these dependencies were excluded to simplify physical relationships and concentrate analyses on the blade flow field. This was done by analyzing measured LFA and C_n in lieu of derived α and C_l.

Normalization of aerodynamic forces also presents challenges. In the current work, normal force was nondimensionalized by local dynamic pressure to obtain C_n. Local dynamic pressure was computed as the difference between test section static pressure (p_∞) and local total pressure. Local

total pressure was sensed at each full pressure tap distribution as the highest pressure in the tap distribution. This methodology for quantifying dynamic pressure has been analyzed previously, and found to induce average errors in dynamic pressure of approximately 1.0 percent.[14]

4. Results and discussion

Analyses began with computation of C_n power spectra for the range of experimental conditions, and identification of principal components present in these spectra. Then, mean flow field structure was considered to gain preliminary understanding of power spectra trends, and as a basis for subsequent analyses intended to furnish more detailed comprehension. Finally, C_n power spectra results were recast in terms of Strouhal number to generalize patterns in principal shedding frequency.

4.1 C_n power spectra

To consistently quantify local blade shedding frequencies, power spectra were computed for C_n time records using a Matlab Fast-Fourier Transform (FFT) algorithm. Prior to computing each FFT, a triangular window was applied to the data record, to minimize introduction of spurious frequency components due to time record initiation/termination. Since experimental measurements were sampled at 520.83 Hz over an acquisition time of 30 seconds, power spectrum resolution was 1/30 Hz. In general, spectra showed negligible power content beyond approximately 60 Hz. Moreover, spectral features of significant magnitude were confined to the range 0 Hz $\leq$ f $\leq$ 20 Hz.

Figure 4 shows a C_n power spectrum for U_∞ = 8 m/s at 0.47R, for the frequency range 0 Hz $\leq$ f $\leq$ 20 Hz. Prominent in Figure 4 are five narrow peaks at f = 1.20, 2.40, 3.60, 4.80, and 6.00 Hz. The magnitudes of these peaks range from 0.033 to 0.197. From these data, it is clear that frequency components corresponding to blade passage were present in the C_n time records.

However, it is important to note that spectral peaks corresponding to blade passage possessed the following pertinent attributes. First, these peaks were fixed and narrow in frequency, indicating that the blade passage frequency varied imperceptibly during data acquisition. Second, the heights of these peaks consistently were one order of magnitude lower than those connected with aerodynamic shedding phenomena studied in the current work. Finally, being narrow and of smaller height, these blade passage peaks contained relatively little spectral power.

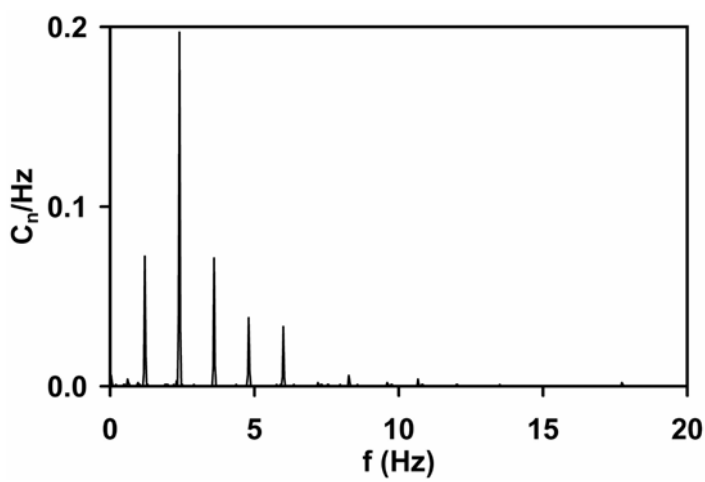

Figure 4. C_n power spectrum for U_∞ = 8 m/s, at 0.47R.

Together, these three attributes indicate point to two crucial implications. First, blade passage spectral features were readily identified and distinguished from aerodynamic shedding features deemed to be of interest herein. Second, blade passage spectral power was small compared to that contained in the aerodynamic shedding phenomena of interest, and thus exerted relatively little influence on principal shedding aerodynamics. The absence of other appreciable spectral content in Figure 4 indicates that C_n unsteadiness due to other sources was negligible under these conditions. The

Figure 4 power spectrum was typical of those observed at 0.30R, 0.47R, 0.67R, and 0.80R, for low test section speeds in the range 5 m/s ≤ U_∞ ≤ 9 m/s.

Figure 5 shows a C_n power spectrum for U_∞ = 11 m/s at 0.47R, again for the frequency range 0 Hz ≤ f ≤ 20 Hz. In this spectrum, two features are readily apparent. The first lies approximately between 1 and 3 Hz, the base of which consists of continuous spectral content extending up to a magnitude of 0.1 to 0.2, which is surmounted by seven sharp peaks. The highest of the seven peaks is located at f = 2.1 Hz and has a magnitude of 0.830. The second feature consists of a sharp peak at f = 6.00 Hz, and has a magnitude of 0.666.

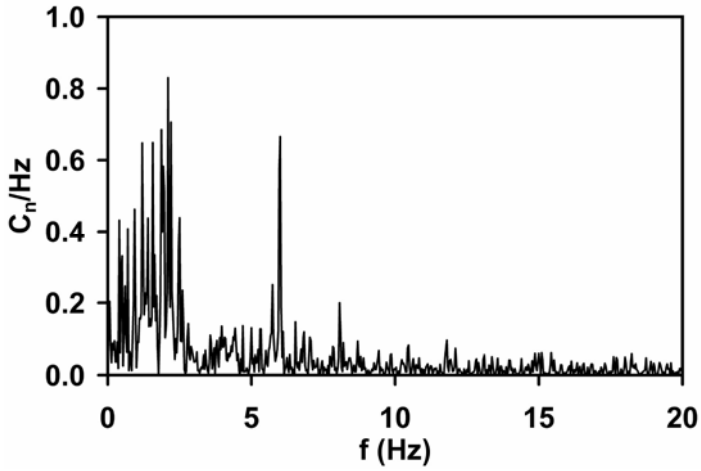

Figure 5. C_n power spectrum for U_∞ = 11 m/s, at 0.47R.

In the Figure 5 power spectrum, the principal frequency was considered to be 2.1 Hz, since the highest sharp peak and the approximate centroid of the base spectral content both were located at 2.1 Hz. Because the second feature at 6.0 Hz was narrow and of smaller magnitude, contained substantially less spectral power, and corresponded to a harmonic of the blade passage frequency, it was not considered pertinent in the current work. The remainder of the spectrum is populated by an irregular distribution of discrete peaks that generally have magnitudes below 0.1. The power spectrum in Figure 5 was typical of those observed across the blade radius for moderate test section speeds in the range 10 m/s ≤ U_∞ ≤ 13 m/s.

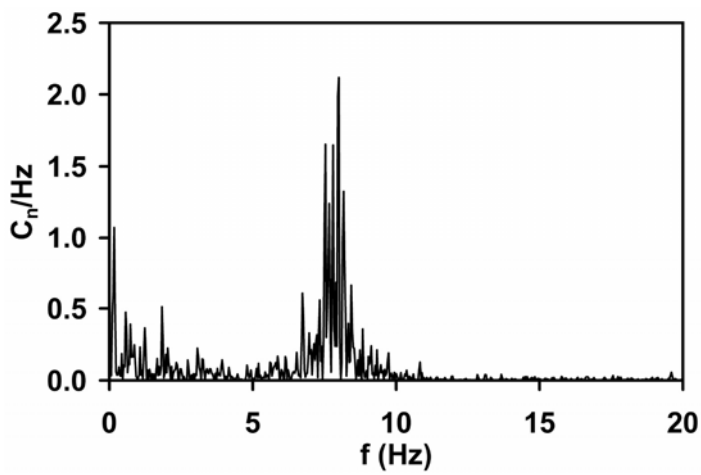

Figure 6. C_n power spectrum for U_∞ = 17 m/s, at 0.47R.

Figure 6 shows a C_n power spectrum for U_∞ = 17 m/s at 0.47R, for the same frequency range as Figures 4 and 5. In Figure 6, one feature clearly dominates the spectrum, and lies in the range 7.4 Hz ≤ f ≤ 8.6 Hz. Similar to the principal feature in Figure 5, the principal feature in Figure 6 has a base of

continuous spectral content and is capped by six sharp peaks. The highest of these six peaks is located at f = 8.0 Hz and has a magnitude of 2.118. Elsewhere in the spectrum, isolated features are present, particularly between 0 Hz and 2 Hz. However, these isolated features have magnitudes of 0.5 to 1.0 and typically are narrow in frequency range, corresponding to very limited C_n spectral power. The power spectrum in Figure 6 was typical of those observed across the blade radius for elevated test section speeds in the range 15 m/s $\leq U_\infty \leq$ 25 m/s.

Using the same criteria described in connection with Figures 5 and 6, principal C_n frequencies

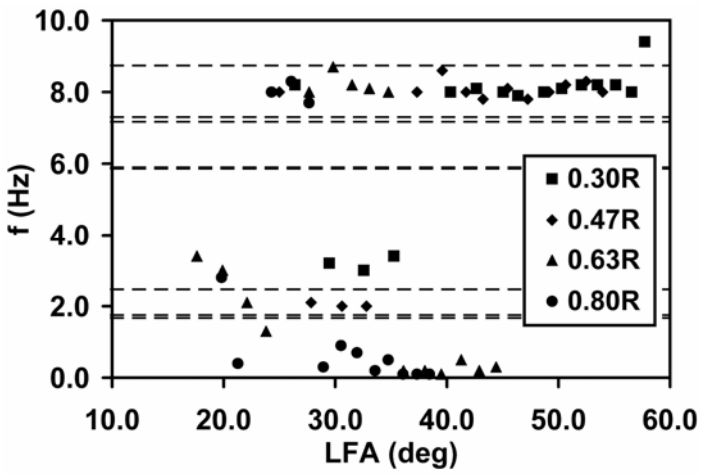

Figure 7. Principal frequencies extracted from C_n power spectra.

corresponding to dominant local blade shedding modes were extracted from C_n power spectra for the experimental range of test section speed and blade radius. These local shedding frequency data are plotted in Figure 7, with respect to local inflow angle (LFA). The resulting data points subdivide into two groups. The upper group extends across 26° $\leq$ LFA $\leq$ 57° in the horizontal direction and 7.7 Hz $\leq$ f $\leq$ 8.7 Hz vertically. The lower group extends across 17° $\leq$ LFA $\leq$ 45° horizontally, and from near zero to 3.4 Hz in the vertical direction.

Also apparent in Figure 7 are eight horizontal dashed lines, located at f = 1.67, 1.75, 2.47, 5.86, 5.90, 7.17, 7.30, and 8.74 Hz, which represent UAE structural resonances identified during modal testing. Modal frequencies 7.17, 7.30, and 8.74 Hz correspond to the asymmetric blade flap mode, symmetric blade flap mode, and the symmetric blade edge mode. Modal testing was carried out with the UAE mounted in the NASA Ames 80 ft x 120 ft wind tunnel, with the rotor parked and at zero test section speed. Structure encompassed by the modal test included the wind tunnel yaw tube, as well as the UAE tower, nacelle, hub, camera boom, blades, and drive train. Within the frequency band 0.5 Hz $\leq$ f $\leq$ 25.5 Hz, 800 spectral lines were resolved, yielding a resolution of 0.031 Hz.[33] Given the spectral resolution achieved in these modal tests and the spectral resolution of the current C_n spectra, no connection is apparent between the aerodynamic shedding modes and the structural resonance modes.

4.2 Mean flow field structure

Figures 8 through 10 show separation/impingement contours superimposed on surface pressure topologies for the rotating blade at U_∞ = 8, 11, and 17 m/s. In all three figures, the blade suction surface planform from 0.25R to 1.00R is depicted, with the upper planform boundary corresponding to the leading edge. Surface pressure contours correspond to Δp = 100 Pa. The separation/impingement contour is represented by the heavy dashed line. Separation/impingement locations were detected by examining mean surface pressure together with standard deviation.[16]

Figure 8 depicts blade surface flow topology for U_∞ = 8 m/s. Pressure contours are closely spaced and extend predominantly in the spanwise direction, indicating that significant chordwise surface pressure gradients are present. This is consistent with flow over the blade surface being attached and

the separation line being situated at the blade trailing edge. With no detectable separation over the blade surface, negligible C_n unsteadiness would be expected, consistent with previous research [19] and with the sparse spectral content observed in Figure 4.

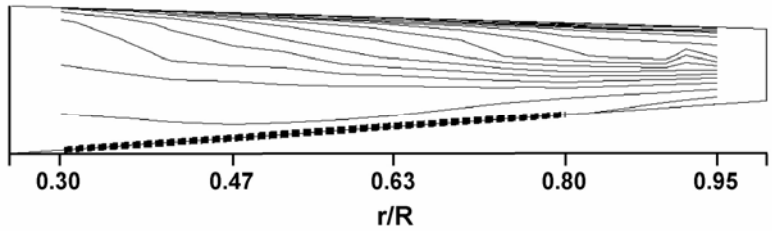

Figure 8. Mean surface pressure contours and separation line for U_∞ = 8 m/s.

Figure 9 shows blade surface flow topology for U_∞ = 11 m/s. Pressure contours still extend mainly in the spanwise direction. However, over the inboard portion of the blade, contours are more sparsely distributed than in Figure 8, which signifies attenuation of chordwise surface pressure gradients. This is consistent with flow over the blade surface being largely separated, with impingement lying at the leading edge at 0.30R and 0.47R, and separation having reached the leading edge at 0.63R and 0.36c at 0.80R. With extensive separation enveloping the blade surface, substantial C_n unsteadiness would be present. This again is consistent with previous research [19] and with the pronounced spectral content observed in Figure 5.

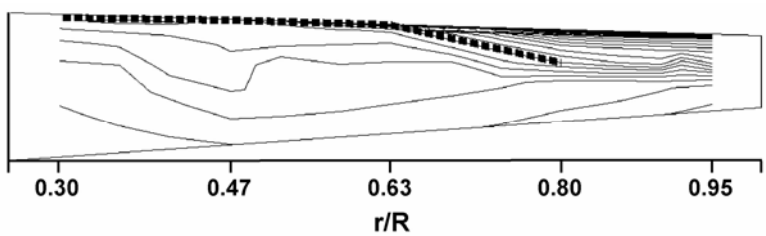

Figure 9. Mean surface pressure contours and impingement/separation line for U_∞ = 11 m/s.

Figure 10 shows blade surface flow topology for U_∞ = 17 m/s. Pressure contours are aligned in the chordwise direction over the forward inboard portion of the blade, and are aligned in the spanwise direction on the aft outboard part of the blade. Surface pressure contours are relatively sparse overall, indicating that flow is separated over the entire blade surface. The impingement contour confirms this, with impingement occurring at the trailing edge at 0.30R, and at 0.56c, 0.20c, and 0.10c at 0.47R, 0.63R, and 0.80R, respectively. At all four radial locations, separation is located at or near the leading edge. Thus, the entire blade surface was separated, and C_n unsteadiness would be of pronounced magnitude.[19] In addition, substantial spectral content would be anticipated, as seen in Figure 6.

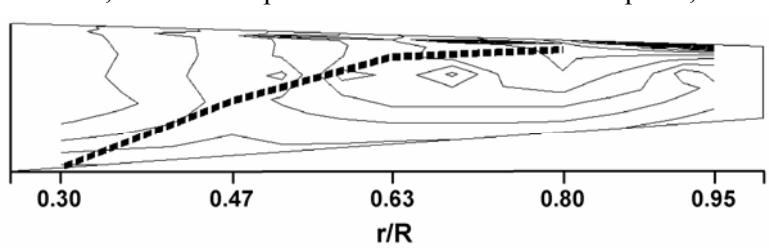

Figure 10. Mean surface pressure contours and impingement line for U_∞ = 17 m/s.

4.3 Strouhal number

Using the information presented above, Strouhal numbers were computed for the C_n shedding frequency data plotted in Figure 7. As shown in the Figure 11 schematic, local inflow speed, U_{loc}, was employed as the characteristic velocity. Because wake width data were not available, projected frontal

height of the local blade chord was adopted as the characteristic dimension, also as shown in Figure 11. This was a plausible approach, since data like those shown in Figures 9 and 10 showed that separation was located at or near the blade leading edge for the shedding frequency measurements in Figure 7. The resulting expression for Strouhal number is shown below as Equation 1.

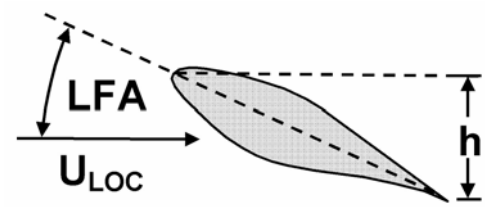

Figure 11. Schematic showing definition of Strouhal number terms.

$$St = \frac{h\,f}{U_{loc}} \qquad (1)$$

The resulting Strouhal number data are shown in Figure 12, and divide unambiguously into three regions on the plot. The first region is bounded by a dashed border and lies near the upper right corner of the plot. Data in this region extend across 37° ≤ LFA ≤ 57° and include Strouhal numbers from 0.12 to 0.18. The second region also is bounded by a dashed line, and is situated near the lower left corner. Data therein span the interval 18° ≤ LFA ≤ 35°, and encompass Strouhal numbers from 0.01 to 0.08. The remaining data points are not demarcated by a border, being lying between 21° ≤ LFA ≤ 45°, and including Strouhal numbers from 0.001 to 0.005.

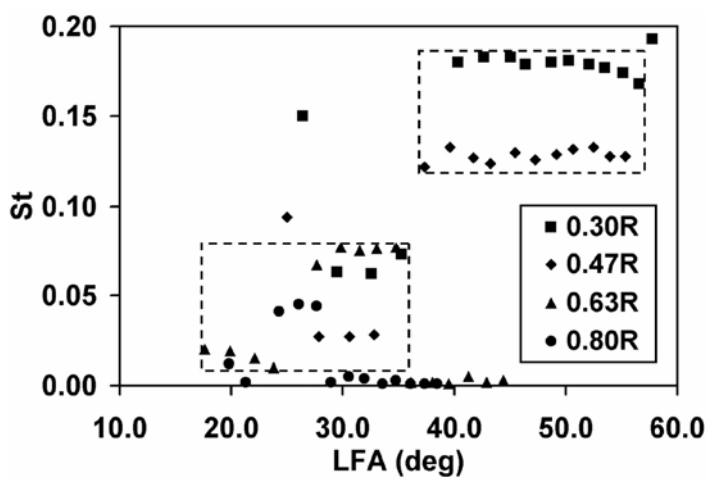

Figure 12. Strouhal numbers for range of experimental measurements.

Correlating the three Strouhal number ranges above with previous research implies that three distinct phenomena are responsible for the observed shedding kinematics. Generally, Strouhal numbers of approximately 0.15 to 0.20 are associated with two-dimensional bluff body vortex shedding that occurs in stall or deep stall conditions. In two-dimensional wind tunnel tests of an S809 airfoil at elevated angles of attack, Swalwell [34] observed Strouhal numbers in the range 0.15 ≤ St ≤ 0.18. Similarities between these previously observed Strouhal numbers and those in the Figure 12 upper right region imply that bluff body vortex shedding occurs on the rotating blade at elevated LFA.

Less conventionally, some investigations have identified Strouhal numbers in the range 0.017-0.032 [35], 0.04-0.06 [36], and 0.076 [37]. These Strouhal number levels occur in the near post-stall regime, and have been associated with three-dimensional surface flow topologies, with periodic

switching between attached and separated conditions, or with singularly high buffet loads. Correspondence between these Strouhal number ranges and that spanned by the lower left region in Figure 12 suggests that three-dimensional flow field structures or periodic mode switching may be present on rotating turbine blades, and may generate elevated fatigue loading. It is interesting to note that the LFA ranges for the lower left region correspond approximately to near post-stall on UAE rotating blade C_n-LFA curves.[15]

Finally, the remaining data points in Figure 12 lie in an extremely low Strouhal number range, from 0.001 to 0.005. At present, no credible physical explanation has been formulated for these data points. However, re-computing these Strouhal numbers using UAE disk diameter as the characteristic dimension instead of blade chord increases Strouhal numbers to approximately 0.10. These Strouhal number levels approach those reported by Medici [38] for wake meandering, which also were computed using disk diameter as the characteristic dimension.

5. Conclusions

Frequency spectra were computed from C_n time series acquired during the NASA Ames wind tunnel experiment, for rotationally augmented flow field conditions at zero yaw. Prominent peaks were present in the frequency spectra, corresponding to dominant aerodynamic shedding modes. These shedding modes were well correlated with flow field mean structure. Strouhal number analyses furnished further information regarding time varying flow field structure responsible for shedding kinematics. The following conclusions can be stated regarding the current study.

At low U_∞ corresponding to low LFA, aerodynamic shedding is negligible, consistent with separation of limited spatial extent. Frequency spectrum artifacts due to blade passage are shown to be small in magnitude, compact in spectral extent, and generally insignificant in the current work.

In the intermediate U_∞ and LFA range, substantial C_n power is concentrated in compact spectral peaks located in the low frequency range. Strouhal numbers imply that aerodynamic shedding in this regime is mediated by three-dimensional flow structures, and may undergo periodic switching between attached and separated conditions, and thus generate singularly high fatigue loads.

As U_∞ and LFA reach elevated levels, considerable C_n spectral power remains focused in compact spectral peaks, but these peaks migrate to higher frequencies. Under these conditions, Strouhal numbers are consistent with bluff body vortex shedding produced by two-dimensional geometries.

This and further investigations will furnish comprehension of the aerodynamics responsible for unsteady load production during rotationally augmented conditions. This, in turn, will help provide a reliable physical basis for accurately predicting the time varying aerodynamic forces responsible for wind turbine fatigue loads and damage.

6. Acknowledgement

The experimental data used in this investigation were acquired from the National Wind Technology Center (NWTC) Unsteady Aerodynamics Experiment (UAE). The wind turbine and instrumentation were designed, fabricated, installed, and maintained by Mr. Jason Cotrell, Mr. Lee Jay Fingersh, and Mr. David Jager. The UAE was installed and tested in the NASA Ames 80 ft x 120 ft National Full-Scale Aerodynamics Complex by these NWTC personnel, with the assistance, advice, and encouragement of numerous NASA Ames engineers, scientists, and technicians.

References

[1] Himmelskamp, H, "Profiluntersuchungen an einem umlaufenden Propeller" ("Profile Investigations on a Rotating Airscrew"), Dissertation, Gottingen 1945; Mitt. Max-Planck-Institut fur Stromungsforschung Gottingen Nr. 2, 1950.

[2] Banks, W., and G. Gadd, "Delaying Effect of Rotation on Laminar Separation," *AIAA J.*, v. 1, n. 4, Apr. 1963, pp. 941-942.

[3] McCroskey, W., and P. Yaggy, "Laminar Boundary Layers on Helicopter Rotors in Forward Flight," *AIAA J.*, v. 6, n. 10, Oct. 1968, pp. 1919-1926.

[4] McCroskey, W. J., "Measurements of Boundary Layer Transition, Separation and Streamline Direction on Rotating Blades," NASA TN D-6321, Apr. 1971.
[5] Madsen, H., and H. Christensen, "On the Relative Importance of Rotational, Unsteady and Three-Dimensional Effects on the HAWT Rotor Aerodynamics*," Wind Engineering*, v. 14, n. 6, 1990, pp. 405-415.
[6] Barnsley, M., and Wellicome, J., "Wind Tunnel Investigation of Stall Aerodynamics for a 1.0 m Horizontal Axis Rotor," *J. of Wind Eng. and Indust. Aerodynamics*, v. 39, 1992, pp. 11-21.
[7] Ronsten, G., "Static Pressure Measurements on a Rotating and a Non-Rotating 2.375 m Wind Turbine Blade. Comparison with 2D Calculations," *J. of Wind Engineering and Industrial Aerodynamics*, v. 39, 1992, pp. 105-118.
[8] Eggers, A., and R. Digumarthi, "Approximate Scaling of Rotational Effects on Mean Aerodynamic Moments and Power Generated by CER Blades Operating in Deep-Stalled Flow," 11th ASME Wind Energy Symposium, Jan. 1992.
[9] Snel, H., R. Houwink, and W. Piers, "Sectional Prediction of 3D Effects for Separated Flow on Rotating Blades," 18th European Rotorcraft Forum, Sept. 1992.
[10] Du, Z., and Selig, M., "A 3-D Stall-Delay Model for Horizontal Axis Wind Turbine Performance Prediction," AIAA-98-0021, Jan. 2001.
[11] Corten, G., "Inviscid Stall Model," Proceedings of the European Wind Energy Conference, July 2001, pp. 466-469.
[12] Tangler, J., and M. Selig, "An Evaluation of an Empirical Model for Stall Delay due to Rotation for HAWTS," NREL/CP 440-23258, Golden, CO: Natl. Renewable Energy Laboratory.
[13] Corrigan, J., and J. Schillings, "Empirical Model for Stall Delay Due to Rotation," American Helicopter Society Aeromechanics Specialist Conf., Jan. 1994.
[14] Schreck, S., and Robinson, M., "Rotational Augmentation of Horizontal Axis Wind Turbine Blade Aerodynamic Response," *Wind Energy*, v. 5, n. 2/3, pp. 133-150, Apr.-Sep. 2002.
[15] Schreck, S., and Robinson, M., "Structures and Interactions Underlying Rotational Augmentation of Blade Aerodynamic Response," AIAA Paper 2003-0520, 2003.
[16] Schreck, S., and Robinson, M., " Boundary Layer State and Flow Field Structure Underlying Rotational Augmentation of Blade Aerodynamic Response," *J. of Solar Energy Engineering*, v. 125, pp. 448-456, Nov. 2003.
[17] Schreck, S., Sørensen, N., and Robinson, M., "Aerodynamic Structures and Processes in Rotationally Augmented Flow Fields," *Wind Energy*, v 10, n 2, March/April 2007, pp. 159-178.
[18] Sørensen, N., Michelsen, J., and Schreck, S., "Navier-Stokes Predictions of the NREL Phase VI Rotor in the NASA Ames 80 ft x 120 ft Wind Tunnel," *Wind Energy*, v. 5, n. 2/3, Apr-Sep 2002, pp. 151-169.
[19] Schreck, S., and Robinson, M., "Rotationally Augmented Flow Structures and Time Varying Loads on Turbine Blades," AIAA-2007-0627, January 2007.
[20] Schreck, S., and Robinson, M. "Unsteadiness in HAWT Blade Aerodynamic Forces and Flow Field Structures During Rotational Augmentation," AIAA-2005-0776, January 2005.
[21] Butterfield, C., W. Musial, and D. Simms, (1992). "Combined Experiment Phase I Final Report*."* NREL/TP-257-4655. Golden, CO: National Renewable Energy Laboratory.
[22] Miller, M., D. Shipley, T. Young, M. Robinson, M. Luttges, and D. Simms (1995), "Combined Experiment Phase II Data Characterization." NREL/TP 442-6916, Golden, CO: National Renewable Energy Laboratory.
[23] Fingersh, L., D. Simms, C. Butterfield, and M. Jenks, "An Overview of the Unsteady Aerodynamics Experiment Phase III Data Acquisition System and Instrumentation," ASME Energy and Environment Expo '95, Houston, TX, Jan.-Feb. 1995.
[24] Acker, T., "Further Analysis of Data from the Unsteady Aerodynamics Experiment, Phase III and Phase IV," Task 2 Report, Subcontr. XAT-8-18211-01, Golden, CO: National Renewable Energy Laboratory.

[25] Hand, M., D. Simms, L. Fingersh, D. Jager, J. Cotrell, S. Schreck, and S. Larwood (2001), "Unsteady Aerodynamics Experiment Phase VI: Wind Tunnel Test Configurations and Available Data Campaigns," NREL/TP-500-29955, Dec. 2001, Golden, CO: Natl. Renewable Energy Lab.
[26] Giguere, P., and M. Selig,"Design of a Tapered and Twisted Blade for the NREL Combined Experiment Rotor," NREL/SR 500-26173, Apr. 1999, Golden, CO: Natl. Renewable Energy Lab.
[27] Zell, P., "Performance and Test Section Flow Characteristics of the National Full-Scale Aerodynamics Complex 80- by 120-Foot Wind Tunnel," NASA TM 103920, Jan 1993.
[28] Brand, A., "To Estimate the Angle of Attack of an Airfoil from the Pressure Distribution," ECN Technical Report, ECN-R-94-002, January 1994.
[29] Schepers, J., "Angle of Attack in Aerodynamic Field Measurements on Wind Turbines," ECN Technical Report, December 1995.
[30] Shipley, D., Miller, M., Robinson, M., and Luttges, M., "Techniques for the Determination of Local Dynamic Pressure and Angle of Attack on a Horizontal Axis Wind Turbine," NREL Technical Report TP-442-7393, May 1995.
[31] Whale, J., Fisichella, C., and Selig, M., "Correcting Inflow Measurements from HAWTs Using a Lifting-Surface Code," AIAA 99-0040, January 1999.
[32] van Bussel, G., "The Aerodynamics of Horizontal Axis Wind Turbine Rotors Explored with Asymptotic Expansion Methods," Thesis Technische Universiteit Delft, The Netherlands, 1995.
[33] Steedman, J., "Modal Test of the Unsteady Aerodynamics Experiment," Navcon Engineering Project 00986, Spring 2000: Navcon Engineering Network, Fullerton, CA (unpublished).
[34] Swalwell, K., "The Effect of Turbulence on Stall of Horizontal Axis Wind Turbines," Ph.D. thesis, Dept. of Mechanical Engineering, Monash University (2005).
[35] Bragg, M., Heinrich, D., Balow, F., and Zaman, K.,"Flow Oscillations over an Airfoil Near Stall," *AIAA Journal*, v. 34, n. 1, pp. 199-201.
[36] Yon, S., and Katz, J.,"Study of the Unsteady Flow Features on a Stalled Wing," AIAA-97-1927, June 1997.
[37] Mabey, D.,"Review of the Normal Force Fluctuations on Aerofoils with Separated Flow," Prog. Aerospace Sci., v. 29, pp. 43-80, 1992.
[38] Medici, D., "Experimental Studies of Wind Turbine Wakes – Power Optimization and Meandering," Doctoral Thesis, KTH Mechanics, Royal Institute of Technology (2005).

REPORT DOCUMENTATION PAGE

Form Approved
OMB No. 0704-0188

The public reporting burden for this collection of information is estimated to average 1 hour per response, including the time for reviewing instructions, searching existing data sources, gathering and maintaining the data needed, and completing and reviewing the collection of information. Send comments regarding this burden estimate or any other aspect of this collection of information, including suggestions for reducing the burden, to Department of Defense, Executive Services and Communications Directorate (0704-0188). Respondents should be aware that notwithstanding any other provision of law, no person shall be subject to any penalty for failing to comply with a collection of information if it does not display a currently valid OMB control number.
PLEASE DO NOT RETURN YOUR FORM TO THE ABOVE ORGANIZATION.

1. REPORT DATE *(DD-MM-YYYY)*
August 2007

2. REPORT TYPE
Conference paper

3. DATES COVERED *(From - To)*
August 28-31, 2007

4. TITLE AND SUBTITLE
Spectral Content and Spatial Scales in Unsteady Rotationally Augmented Flow Fields: Preprint

5a. CONTRACT NUMBER
DE-AC36-99-GO10337

5b. GRANT NUMBER

5c. PROGRAM ELEMENT NUMBER

6. AUTHOR(S)
S.J. Schreck

5d. PROJECT NUMBER
NREL/CP-500-41744

5e. TASK NUMBER
WER7.2601

5f. WORK UNIT NUMBER

7. PERFORMING ORGANIZATION NAME(S) AND ADDRESS(ES)
National Renewable Energy Laboratory
1617 Cole Blvd.
Golden, CO 80401-3393

8. PERFORMING ORGANIZATION REPORT NUMBER
NREL/CP-500-41744

9. SPONSORING/MONITORING AGENCY NAME(S) AND ADDRESS(ES)

10. SPONSOR/MONITOR'S ACRONYM(S)
NREL

11. SPONSORING/MONITORING AGENCY REPORT NUMBER

12. DISTRIBUTION AVAILABILITY STATEMENT
National Technical Information Service
U.S. Department of Commerce
5285 Port Royal Road
Springfield, VA 22161

13. SUPPLEMENTARY NOTES

14. ABSTRACT *(Maximum 200 Words)*
This paper describes the spatial and temporal attributes of the structures and processes present in wind turbine flow fields hold important implications for load predictions for turbine design and analysis, as well as active aerodynamic control methodologies currently being considered for wind turbine applications.

15. SUBJECT TERMS
wind energy; wind turbine design; aerodynamic design

16. SECURITY CLASSIFICATION OF:			17. LIMITATION OF ABSTRACT	18. NUMBER OF PAGES	19a. NAME OF RESPONSIBLE PERSON
a. REPORT	b. ABSTRACT	c. THIS PAGE			19b. TELEPHONE NUMBER (*Include area code*)
Unclassified	Unclassified	Unclassified	UL		

Standard Form 298 (Rev. 8/98)
Prescribed by ANSI Std. Z39.18

F1147-E(12/2004)